Journal of Solid State Chemistry **164,** 246–251 (2002)
doi:10.1006/jssc.2001.9469, available online at http://www.idealibrary.com on IDEAL®

New 4234-type Intermetallic Borocarbides: Synthesis, Structure, and Magnetic Properties

J. R. Link,* S. M. Loureiro,* C. Kealhofer,* H. W. Zandbergen,*,† and R. J. Cava*

*Department of Chemistry and Princeton Materials Institute, Princeton University, Princeton, New Jersey 08544; and †Laboratory for Materials Science, Delft University of Technology, 2628 Al Delft, The Netherlands

Received June 27, 2001; in revised form November 13, 2001; accepted November 30, 2001; published online January 31, 2002

New 4234-type compounds, structurally related to the $n = 4$ member of the $(LnC)_nNi_2B_2$ homologous series of intermetallic borocarbides, were synthesized by arc-melting. Here we report that this structure type, previously observed only for Ni-based compounds, can be synthesized for a large number of transition elements. Further, we find it to be stable for medium through small lanthanides. The compounds have formulas $Y_4T_2B_3C_4$ [T = Fe, Co, Ni, Ru, Rh, and Ir], $Ln_4T_2B_3C_4$ [Ln = Er, Dy, and Gd; T = Fe and Co], $Lu_4Ni_2B_3C_4$, and $Sc_4Ni_2B_3C_4$. The unit cells are pseudo-tetragonal, with lattice parameters ranging from $a = 3.348(1)$ Å, $c = 25.90(1)$ Å for $Sc_4Ni_2B_3C_4$ to $a = 3.624(1)$ Å, $c = 26.63(1)$ Å for $Y_4Rh_2B_3C_4$. Structural investigation by exit-wave reconstruction is reported, showing the presence of twinning on the unit cell scale. The phases show either Curie–Weiss behavior with very small magnetic moments per transition metal atom or temperature-independent paramagnetism. © 2002 Elsevier Science (USA)

INTRODUCTION

Before the recent discovery of superconductivity in MgB_2 (1), the quaternary borocarbides, with superconducting temperatures (T_c) reaching 23 K for YPd_2B_2C (2–7), had sparked a renewed interest in the chemistry and physics of intermetallic superconductors. A homologous series of compounds has previously been reported for the Ni-based materials. The series, which consists of stacking of LnX [100] rocksalt-type layers, and Ni_2B_2 layers of edge-shared NiB_4 tetrahedra, has the general formula $(LnX)_nNi_2B_2$ (8). For the borocarbides, X = C, $n = 1$, 2, and 4 are known, and for boronitrides, X = N, $n = 2$ and 3 are known. The $n = 1$ compound $LuNi_2B_2C$ is superconducting at 16 K, the $n = 2$ compound YNiBC is superconducting below 9 K on partial substitution of Cu for Ni (9), and the $n = 3$ compound $La_3Ni_2B_2N_3$ is superconducting at 13 K (10, 11). The $n = 4$ compound, previously observed only for the Ni borocarbides (12), is not superconducting, and has been little studied.

The $n = 4$ "4234" phase (the numbers in the shorthand nomenclature refer to subscripts in the chemical formula) was initially found in searches for possible higher stacking sequences in the $(LnC)_nNi_2B_2$ homologous series. This fourth member of the series was initially reported to have the formula Ln_2NiBC_2 ($Lu_4Ni_2B_2C_4$) (12), but further investigation indicated that the actual composition was $Lu_4Ni_2B_3C_4$ (13). The crystal structure of this phase, which has monoclinic symmetry but is pseudo-tetragonal, has not yet been exactly solved due to what we show here to be severe unit cell scale twinning of the crystallites. Previous transmission electron microscopy studies have shown that the structure is related to that expected for the ideal $n = 4$ member of the borocarbide superconductor family with an additional boron layer inserted between the two inner LnC rocksalt-type layers in the four-layer rocksalt-like structural component. The stacking of layers is $(Ni_2B_2)(LnC)(LnC)(B)(LnC)(LnC)(Ni_2B_2)(LnC)(LnC)(B)(LnC)(LnC)\ldots$. A structural model of the 4234 phase based on electron microscopy structural images is shown in Fig. 1.

Electronic band structure calculations for the $LuNi_2B_2C$ ($n = 1$) superconductor revealed a high density of states at the Fermi level in an electronic band dominated by in-plane orbital overlap of Ni d states (14–17). These calculations showed for LuNiBC that it might be possible to dope higher stacking members to render them superconducting if a sufficient number of electrons could be added to the compound to fill the same orbital populated in the $n = 1$ phase. This was eventually realized in $YNi_{1-x}Cu_xBC$ (9). The search for superconductivity in higher stacking of LnX layers was actively pursued in the years following the discovery of the superconducting borocarbides, resulting in the discovery of superconductivity in $La_3Ni_2B_2N_3$, but $Lu_4Ni_2B_3C_4$ was not found to be superconducting.

To broaden the research on these phases and to potentially find superconductivity in other families of intermetallic borocarbides, we have synthesized 12 new 4234 phases. We report here their synthesis and magnetic properties. Surprisingly, we find that despite its apparent structural

0022-4596/02 $35.00

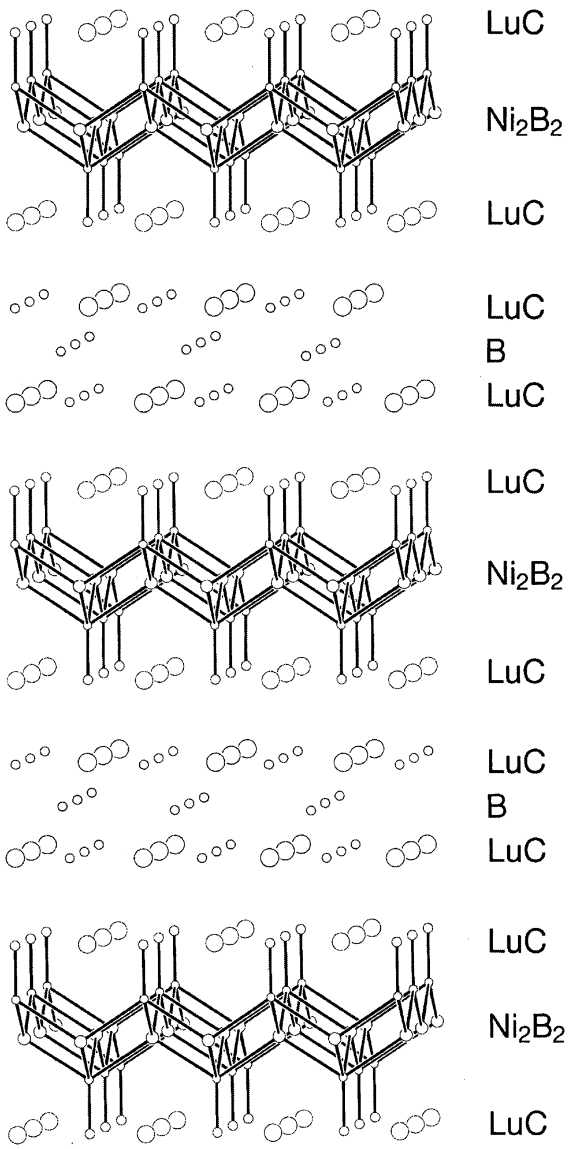

FIG. 1. Structural model for the 4234-type phase. The large and small open circles in the LuC layer indicate lutetium and carbon atoms, respectively. The Ni_2B_2 layer shows the coordination of nickel atoms in the NiB_4 tetrahedra. The distinct intermediate boron layer can be seen between two central LuC layers.

complexity, this 4234 structure type is, by far, found for a wider range of transition metals than any other structure type in the quaternary borocarbide family, suggesting that it represents a very stable intermetallic structure type. We report that the phase can be made for Co-, Fe-, Ru-, Rh-, and Ir-based compounds as well as for Ni, indicating its stability for a wide range of electron counts.

EXPERIMENTAL

Stoichiometric amounts of high-purity grade lanthanide metal shavings or sublimed dendrites, transition metals, and coarse carbon and boron powders were mixed, pressed into pellets, and arc-melted under argon. The resulting buttons were melted three times. Weight loss on melting was less than 2%. Annealing the samples by wrapping in tantalum foil, sealing in SiO_2 tubes under vacuum, and annealing at

TABLE 1
Pseudotetragonal Lattice Parameters for the 4234 Quaternary Borocarbides

Composition	a (Å)	c (Å)
$Sc_4Ni_2B_3C_4$	3.348(1)	25.90(1)
$Y_4Fe_2B_3C_4$	3.569(1)	27.15(1)
$Y_4Co_2B_3C_4$	3.568(1)	26.63(1)
$Y_4Ni_2B_3C_4$	3.475(1)	26.73(1)
$Y_4Ru_2B_3C_4$	3.581(1)	27.39(1)
$Y_4Rh_2B_3C_4$	3.624(1)	26.63(2)
$Y_4Ir_2B_3C_4$	3.619(1)	26.95(1)
$Er_4Fe_2B_3C_4$	3.519(1)	27.00(1)
$Er_4Co_2B_3C_4$	3.530(1)	26.37(1)
$Dy_4Fe_2B_3C_4$	3.574(2)	26.41(2)
$Dy_4Co_2B_3C_4$	3.574(2)	26.37(1)
$Gd_4Fe_2B_3C_4$	3.602(2)	27.21(2)

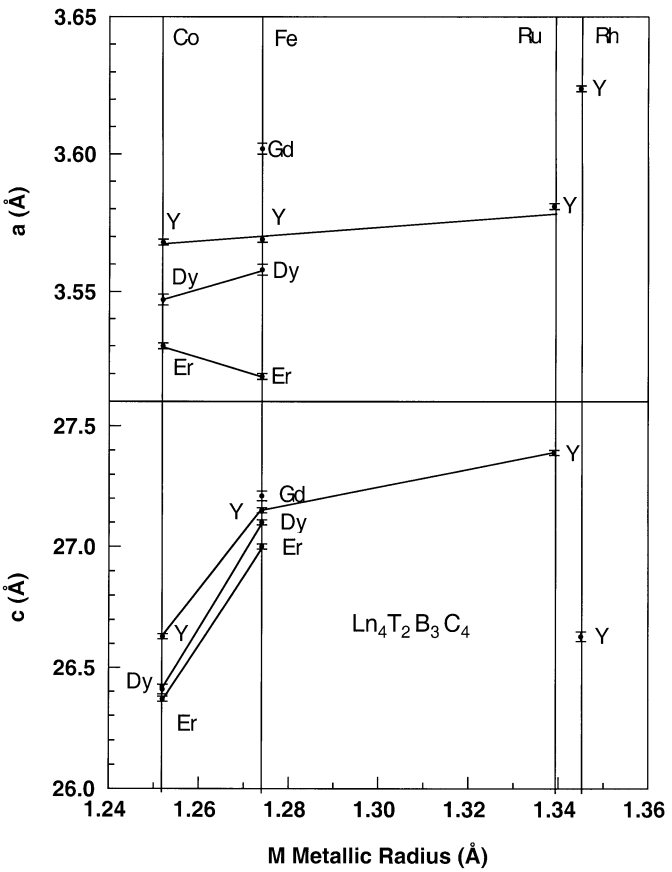

FIG. 2. Lattice parameters a (top) and c (bottom) for several 4234-type phases. The vertical lines indicate the T transition metal.

temperatures between 900°C and 1100°C did not improve sample purity. This suggests congruent or nearly congruent melting of the compounds, or stability at temperatures above 1100°C. Therefore, as-melted samples were employed in all analyses. Several new phases were synthesized through this process: $Y_4T_2B_3C_4$ [T = Fe, Co, Ni, Ru, Rh, and Ir] and $Ln_4T_2B_3C_4$ [Ln = Er, Dy, and Gd; T = Fe and Co]. The new phase $Sc_4Ni_2B_3C_4$ was also obtained in this study, as well as the previously reported $Lu_4Ni_2B_3C_4$, whose physical properties had not been measured. Although we did not synthesize all possible lanthanide–transition metal combinations, this phase is likely to be stable for all heavy lanthanides for the transition metals Ni, Co, Fe, Rh, Ir, and Ru.

X-ray powder diffraction was carried out using a Rigaku Miniflex powder diffractometer with Cu$K\alpha$ radiation ($\lambda = 1.54056$ Å) at room temperature. Thin specimens for electron microscopy were obtained by crushing under dry isopropanol and mounting the crystal fragments on a Cu grid covered with a carbon-coated holey film. Electron microscopy was performed with a Philips CM30ST-FEG electron microscope. For the through-focus exit-wave reconstruction (TF-EWR), series of 15–20 HREM images were recorded with focus increments of 5.2 nm. These series were recorded with a 1024×1024 pixel Photometrix CCD camera with a dynamic range of 12 bits. In the exit-wave reconstruction, developed by Van Dyck and Coene (18), all useful information is extracted from a series of HREM images taken at different defocus values with known focus increments. The result is that the exit wave contains amplitude as well as phase information up to the information limit of the microscope. A major advantage of the exit wave is that the information, which is delocalized in the HREM images resulting in a blurred image (19), is restored to its origin. In addition to the advantage of the deblurring, the noise level of the exit wave is less than for a single image since 15–20 HREM images are used for the reconstruction. The magnetic properties were measured with a Quantum Design PPMS magnetometer on bulk pieces of the synthesized polycrystalline samples.

RESULTS AND DISCUSSION

X-ray powder diffraction for all samples except the materials noted below showed clean patterns of the 4234 phase with no visible impurities. Samples of composition

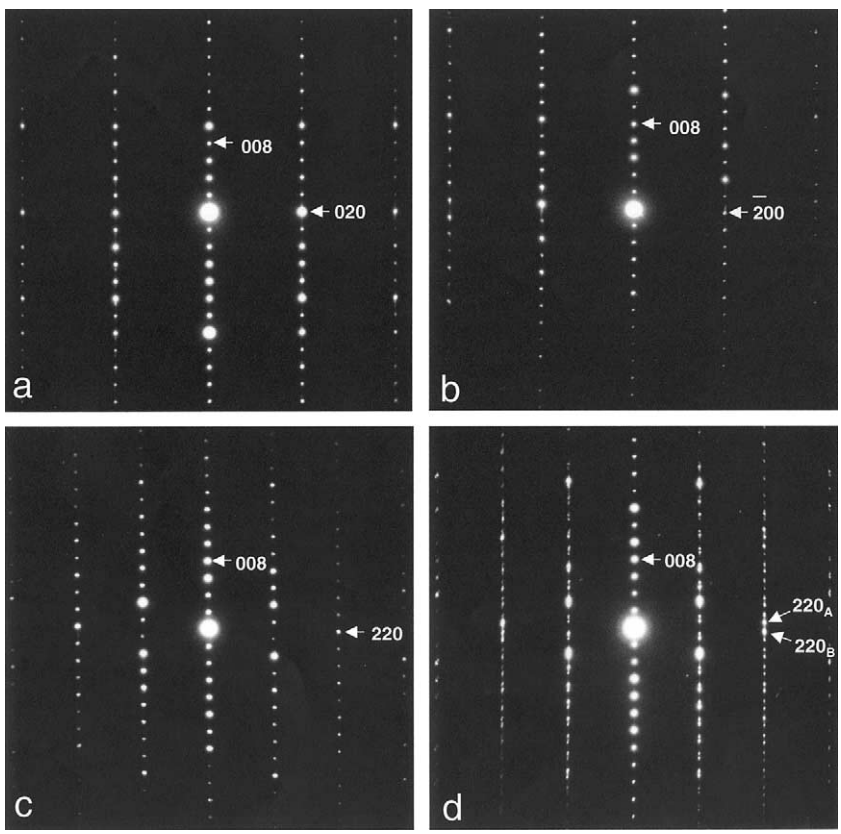

FIG. 3. Electron diffraction patterns of $Lu_4Ni_2B_3C_4$ along (a) [100], (b) [010], and (c) [110]. (d) shows a diffraction pattern with streaking due to the twinning. Note that the streaking is not present along the line of the 001 reflections, indicating that there is no significant deviation of the stacking sequence of the layers.

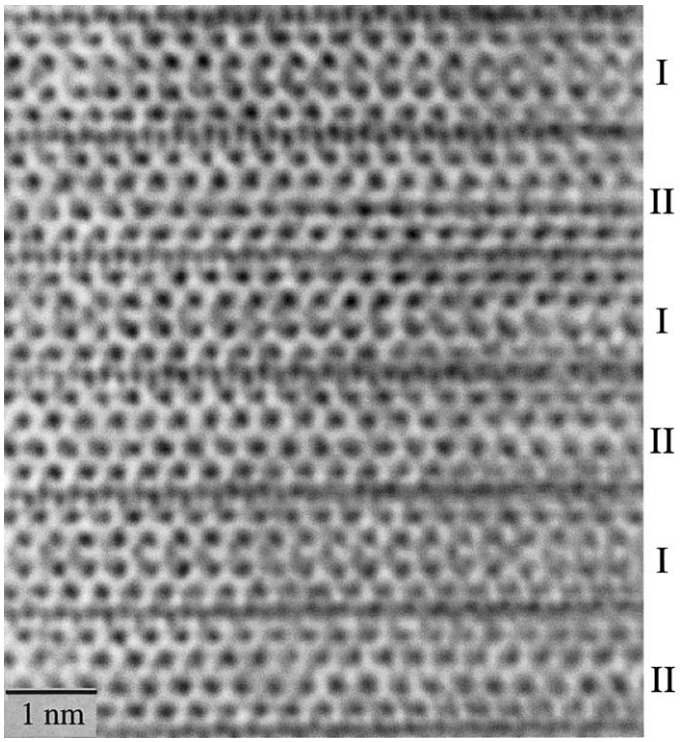

FIG. 4. Reconstructed exit wave (amplitude) of $Lu_4Ni_2B_3C_4$, showing different kinds of stacking: *ABBA* (indicated by I) and *ABAB* (indicated by II). These stackings are visible in the [110] and [1–10], zones, respectively.

$Y_4Ir_2B_3C_4$, $Sc_4Ni_2B_3C_4$, and $Er_4Fe_2B_3C_4$, while greater than approximately 80% 4234 phase, however, showed some unidentified impurity phases. The diffraction patterns could be indexed at low diffraction angles on a pseudo-tetragonal cell, with $a \approx 3.6$ Å, $c \approx 27$ Å, consistent with the electron diffraction analysis of $Lu_4Ni_2B_2C_4$. The pseudo-tetragonal lattice parameters of the phases obtained are presented in Table 1 and are shown in Fig. 2 as a function of the metallic radius of the transition metal (20). The vertical lines indicate the transition metal T, where $T =$ Co, Fe, Ru, and Rh. For the same transition metal, the lattice parameters increase with increasing metallic radius of the lanthanide cation. For the same lanthanide, as a general trend, the lattice parameters also increase with increasing radius of T. The exception is erbium, for which the a-parameter in $Er_4Fe_2B_3C_4$ is slightly smaller than that of $Er_4Co_2B_3C_4$. For adjacent metals, such as Ru and Rh, the a-parameter is much smaller, and the c-parameter is much larger for $Y_4Ru_2B_3C_4$ than for $Y_4Rh_2B_3C_4$. The phase $Sc_4Ni_2B_3C_4$ has much smaller lattice parameters than the other analogues [$a = 3.348(1)$ Å, $c = 25.90(1)$ Å], due to the smaller metallic radius of scandium.

Electron diffraction was carried out with a number of crystals of $Lu_4Ni_2B_3C_4$, which were rotated to scan the reciprocal space. This indicated that the true unit cell is A-centered monoclinic, with $a \approx 5.0$ Å, $b \approx 5.0$ Å, $c \approx 27.4$ Å, $\alpha \approx 93°$. Electron diffraction patterns of the [100], [010], and [110] orientations are given in Fig. 3. In a number of crystals extra spots and some streaking could be observed along the c*-axis (see Figs. 3a–3d). These extra spots and streaking occur, however, not along the line of the 001 reflections, indicating that there is no significant deviation of the stacking sequence of the layers but that layers may only be shifted in the (001) plane with respect to each other. The monoclinic angle varies somewhat from crystal to crystal and also within a given crystal. In general the [110] diffraction patterns showed twinning like in Fig. 3d. Figure 4 shows a reconstructed exit wave in which the Lu atoms and the Ni atoms appear as black dots. Two types of stacking of the Lu atoms along the c-axis can be seen: an *ABBA* stacking and an *ABAB* stacking. These two stacking types occur because there are two ways in which the two LuC layers neighboring the B layer are shifted with respect to each other, as shown in Fig. 5. This mixture of *ABBA* and *ABAB* stacking on the unit cell and nanometer level occur in all crystals investigated. Another example of this is shown in Fig. 6. The imaging conditions are chosen such that the *ABBA* stacking is clearly seen whereas the *ABAB* stacking is only fuzzy. Also, twinning resulting in interchange between the a-axis and the b-axis can be observed, as is shown in Fig. 7. In this figure, a white line indicates the c-direction. This white line changes direction, indicating a change in the monoclinic angle. In some areas the angle is almost 90°, suggesting that these areas are in the [100] orientation. In the area indicated with the white arrow a defect is present,

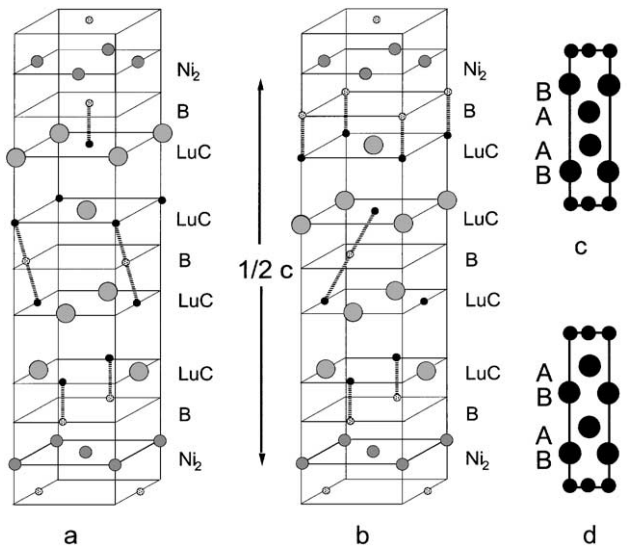

FIG. 5. Schematic representation of the basic stacking of the LuC–LuC–B–LuC–LuC blocks. (a) and (b) show half the unit cell of $Lu_4Ni_2B_3C_4$ for two stackings, which are actually the same stacking but viewed along the [110] and [1–10] directions, respectively. (c) and (d) show the resulting black dot patterns in the HREM images for the stacking in (a) and (b), respectively.

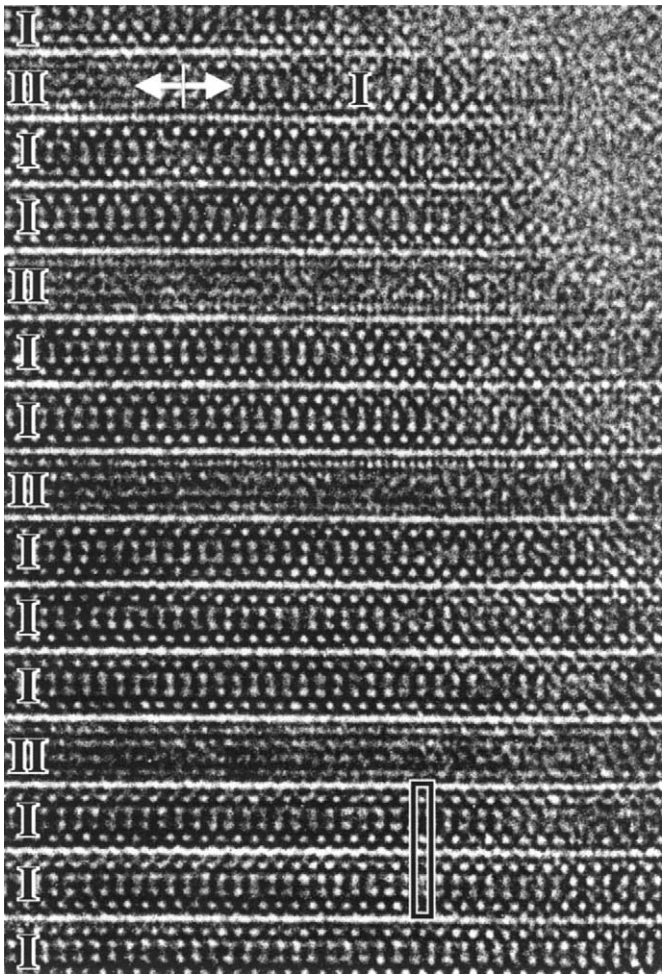

FIG. 6. A [110]/[1–10] micrograph taken at defocus values of about − 70 nm showing the existence of two types of structure images stacked in a randomized way. The two types are labeled I (*ABBA*) or II (*ABAB*). At the top of the image a transformation from an I to an II type of stacking (indicated by the arrows) can be seen. The projection of the unit cell is indicated by a box.

which is due to the difference in direction of the *c*-axis on both sides.

The temperature dependence of the magnetic susceptibility, $\chi(T)$, measured at 5 T, showed that several of the materials follow Curie–Weiss behavior. In this group are included $Y_4Ni_2B_3N_4$, $Y_4Ru_2B_3C_4$, $Y_4Rh_2B_3C_4$, and $Y_4Ir_2B_3C_4$, (Fig. 8, upper panel). The magnetic moments found are very low—on the other order of 0.20 μ_B/mol transition metal atom. The temperature-independent part of the magnetic susceptibility has the same order of magnitude for the latter four compositions, and on the order of 10^{-5} emu/mol. The Curie–Weiss temperature is slightly negative, ranging from − 7 K for $Y_4Ru_2B_3C_4$ to − 19 K for $Y_4Ni_2B_3C_4$, indicating very weak antiferromagnetic interactions. The very low moments for these phases may be due to the presence of very small amounts of paramagnetic impurities or may be intrinsic to the phases. No magnetic ordering was observed in these cases at temperatures above 4 K. $Lu_4Ni_2B_3C_4$ and $Sc_4Ni_2B_3C_4$ samples showed basically temperature-independent paramagnetism (Fig. 8, lower panel).

The $Gd_4Fe_2B_3C_4$, $Dy_4Fe_2B_3C_4$, $Y_4Fe_2B_3C_4$, and $Y_4Co_2B_3C_4$ samples showed small amounts of ferromagnetism, which would not be a surprising property given the elements present. The largest magnetization observed at room temperature was 8000 emu/mol at a field of 9 T for $Gd_4Fe_2B_3C_4$. It is not clear at this time whether the observed ferromagnetism is intrinsic or extrinsic, as many highly magnetic phases are known in these systems which might be present in small amounts. Further research into the potential magnetic properties of these phases may be of interest.

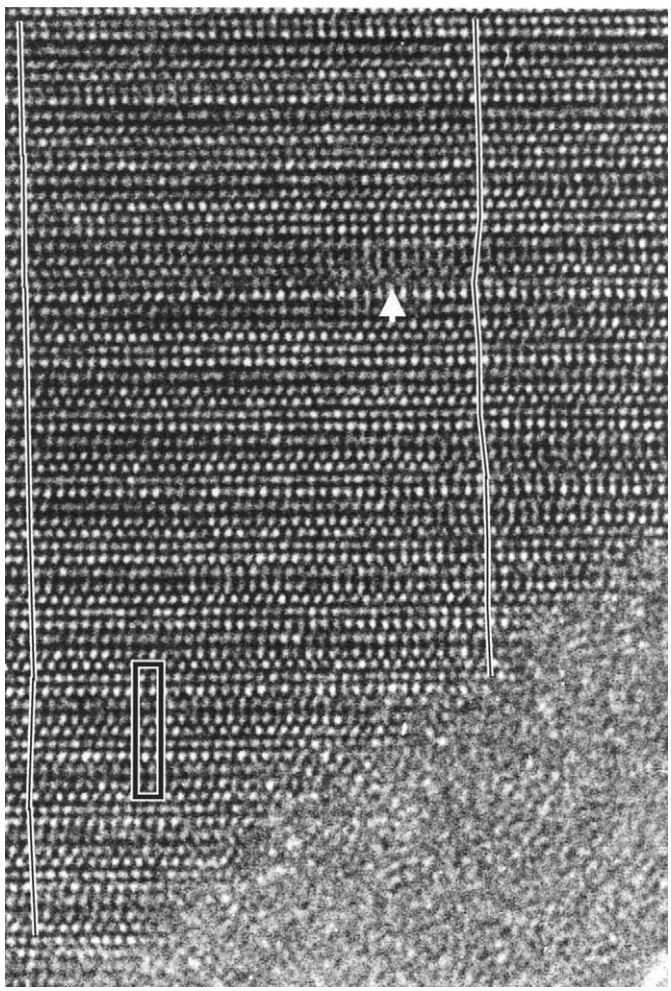

FIG. 7. A [010]/[100] HREM image showing the twinning leading to a change in the direction of the *c*-axis, as indicated by the white lines. The arrow indicates a distortion of the lattice, which is not related with a dislocation, since no Burgers loop is present, but must be due to twinning within the *ab* plane. The amorphous edge in the lower right corner of the image is the result of reaction with air. The unit cell is indicated by a box.

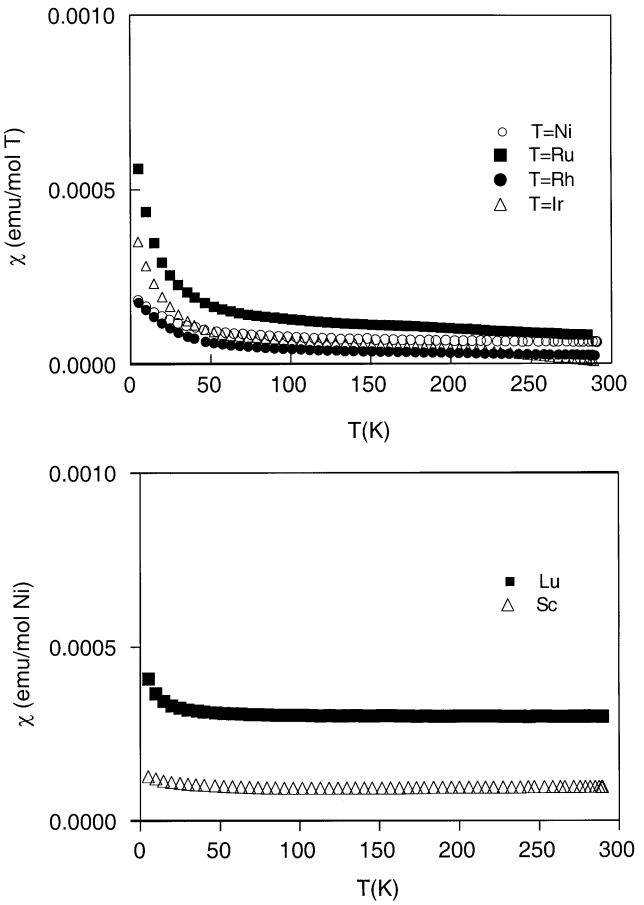

FIG. 8. Magnetic susceptibility data for 4234 samples $Y_4Ni_2B_3C_4$, $Y_4Ru_2B_3C_4$, $Y_4Rh_2B_3C_4$, and $Y_4Ir_2B_3C_4$ (upper panel), and $Lu_4Ni_2B_3C_4$ and $Sc_4Ni_2B_3C_4$ (lower panel), measured at 5 T.

CONCLUSIONS

Several new intermetallic borocarbide phases were synthesized by arc-melting. The phases are monoclinic but have pseudo-tetragonal symmetry, and form for a variety of transition metals and lanthanides. It is surprising that this $Ln_4T_2B_3C_4$ structure type is the most stable in the quaternary borocarbides. It is observed, for example, for T = Fe and Ru, although no other quaternary borocarbides with lower n values (which would have simpler crystal structures) are observed for these transition metals. This is especially surprising, as the general rule for homologous series is that the larger n stacking variants are more unstable than their lower n counterparts. This must be due to the fact that in this case the $(LnC)_2B(LnC)_2$ sandwich, and in particular, the C–B–C unit, is highly thermodynamically stable. Even though the phases are not superconducting as yet, several show weak Curie–Weiss behavior or temperature-independent paramagnetism, and no magnetic ordering, indicating that any tendency toward transition metal-based magnetism in this structure type is very weak or nonexistent. Further studies on different compositions or substitution in these phases may render them superconducting. Though the exact structure of these compounds is not known, electronic structure calculations would be of interest to determine what electron count would be necessary to fill the bands to the level appropriate to induce superconductivity.

ACKNOWLEDGMENTS

The Department of Energy funded this research under grant number DE-FG02-98-ER45706. S.M.L. thanks JNICT/PRAXIS XX/BPD18834/98.

REFERENCES

1. J. Nagamatsu, N. Nakagawa, Y. Z. Murakana, and V. Akimitsu, *Nature* **410,** 63 (2001).
2. P. C. Canfield, P. L. Gammel, and D. J. Bishop, *Phys. Today* **51,** 40 (1998).
3. G. Hilscher and H. Michor, *in* "Studies of High temperature superconductors" (A.V. Narlikar, Ed.), Vol. 28, p. 241. Nova Science Publishers, New York, 1999.
4. C. Godart, E. Alleno, E. Tominez, L. C. Gupta, R. Nagarajan, Z. Hossain, J. W. Lynn, P. Bonville, J. A. Hodges, J. P. Sanchez, and I. Felner, *J. Solid State Chem.* **133,** 169 (1997).
5. R. J. Cava, H. Takagi, H. W. Zandbergen, J. J. Krajewski, W. F. Peck, Jr., T. Siegrist, R. B. van Dover, R. J. Felder, K. Mizuhashi, J. O. Lee, H. Eisaki, and S. Uchida, *Nature* **367,** 146 (1994).
6. R. Nagarajan, C. Mazumdar, Z. Hossain, S. K. Dhar, K. V. Gopalakrishnan, L. C. Gupta, C. Godart, B. D. Padalia, and R. Vijayaraghavan, *Phys. Rev. Lett.* **72,** 274 (1994).
7. R. J. Cava, H. Takagi, B. Batlogg, H. W. Zandbergen, J. J. Krajewski, W. F. Peck, Jr., R. B. van Dover, R. J. Felder, T. Siegrist, K. Mizuhashi, J. O. Lee, H. Eisaki, S. A. Carter, and S. Uchida, *Nature* **367,** 252 (1994).
8. T. Siegrist, H. W. Zandbergen, R. J. Cava, J. J. Krajewski, and W. F. Peck, Jr., *Nature* **367,** 254 (1994).
9. A. K. Gangopadhyay, A. J. Schuetz, and J. S. Schilling, *Physica C* **246,** 317 (1995).
10. R. J. Cava, H. W. Zandbergen, B. Batlogg, H. Eisaki, H. Takagi, J. K. Krajewski, W. F. Peck, Jr., E. M. Gyorgy, and S. Uchida, *Nature* **372,** 245 (1994).
11. H. W. Zandbergen, J. Jansen, R. J. Cava, J. J. Krajewski, and W. F. Peck, Jr., *Nature* **372,** 759 (1994).
12. H. W. Zandbergen, R. J. Cava, J. J. Krajewski, and W. F. Peck, Jr., *J. Solid State Chem.* **110,** 196–199 (1994).
13. H. W. Zandbergen, D. Tang, J. Jansen, and R. J. Cava, *Ultramicroscopy* **64,** 231 (1996).
14. L. F. Matheiss, *Phys. Rev. B* **49,** 13279 (1994).
15. D. J. Singh, *Solid State Commun.* **98,** 899 (1996).
16. W. Pickett and J. D. Singh, *Phys. Rev. Lett.* **72,** 3702 (1994).
17. M. Divis, K. Schwarz, P. Blaha, G. Hilscher, H. Michor, and S. Khmelevskyi, *Phys. Rev. B* **62,** 6774 (2000).
18. W. Coene, G. Janssen, M. Op De Beeck, and D. Van Dyck, *Phys. Rev. Lett.* **69,** 3743 (1992).
19. H. W. Zandbergen and D. Van Dyck, *Microsc. Res. Tech.* **49,** 3 (2000).
20. Metallic radii taken from E. Teatum, K. Gschneider, J. Waber, Compilation of calculated data useful in predicting metallurgical behavior of the elements in binary alloy systems, LA-2345, Los Alamos Scientific Laboratory, Los Alamos, NM, 1960.